ELSA: A foot-size powered prosthesis reproducing ankle dynamics during various locomotion tasks

François Heremans[1], Jeanne Evrard[1], David Langlois[2], Renaud Ronsse[1]

***Abstract*—Powered ankle-foot prostheses offer the potential to emulate natural locomotion dynamics, thereby addressing the issues related to uneven gait and insufficient propulsion typically experienced by individuals with lower-limb amputation wearing a passive prosthetic device. Despite significant progress, existing powered prostheses are often hindered by their substantial build height, bulky design, excessive weight, and noise level, limiting their widespread adoption. This work presents ELSA (Efficient and Lightweight Spring Ankle), a lightweight (1.15 kg) and compact (11 cm high) powered ankle-foot prosthesis fitting within the volume of a shoe and capable of providing a net positive mechanical energy over the gait cycle. This level of integration is achieved through an innovative arrangement of a spring and actuator mechanisms operating in synergy. This hybrid architecture offers users the choice to (i) walk actively, with propulsive energy assistance; (ii) regeneratively, potentially allowing for energy harvesting to recharge the device battery; or (iii) completely turned off (passive). This prototype has been validated during benchtop experiments and through trials involving four amputated participants. These tests encompassed various scenarios, including treadmill walking and everyday ambulation tasks. Additionally, a sensitivity analysis was conducted to assess how different control parameters impacted the provided mechanical energy and resulting gait performance.**

***Index Terms*—Wearable robots, Prosthetics and Exoskeletons, Compliant Joint/Mechanism, Mechanism Design**

I. Introduction

The world is currently facing a rising prevalence of lower-limb amputations, primarily attributed to peripheral vascular diseases, notably diabetes mellitus [1]–[3]. Individuals who have experienced lower-limb loss face significant challenges concerning their mobility and overall quality of life [4]. To overcome this limitation, they are fitted with prostheses replacing their missing limb. However, the vast majority of these devices are passive in the sense that they cannot provide the net positive energy required during daily life ambulation activities like overground walking. To compensate for this lack of propulsion, people with amputation often overexert their remaining joints, which frequently leads to the development of osteoarthritis [5]. Moreover, the reduction in muscle strength following amputation causes an additional burden in terms of propulsion and balance [6], [7]. The altered biomechanics also contributes to an asymmetric gait inducing back pain for a majority of individuals [8].

[1]Institute of Mechanics, Material and Civil Engineering, Louvain Bionics, UCLouvain, Place du Levant 2, L05.04.02, 1348 Louvain-la-Neuve, Belgium
[2]R&D, Össur, Grjótháls 5, 110 Reykjavík, Iceland
F.H. and J.E. contributed equally to this work. F.H is the corresponding author. E-mails: francois.heremans@uclouvain.be, jeanne.evrard@uclouvain.be, dlanglois@ossur.com and renaud.ronsse@uclouvain.be

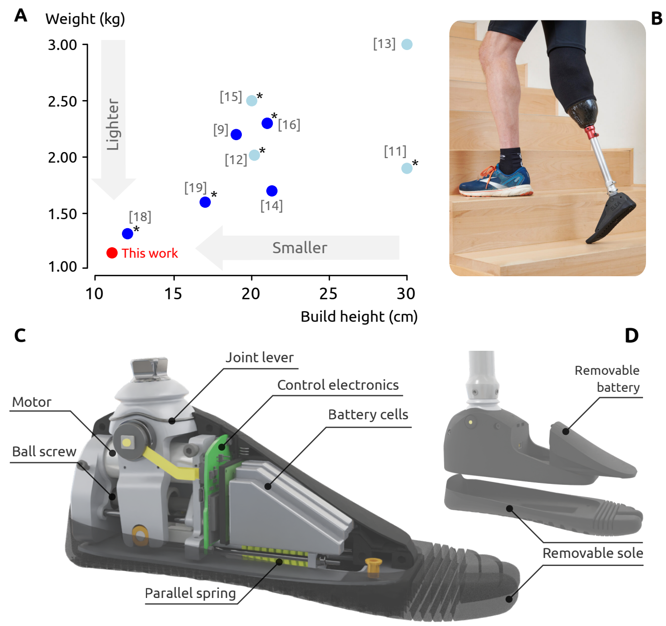

Fig. 1. **A** Comparison between ELSA and several powered ankles from the literature in terms of build height and weight. Light blue dots indicate that we had to estimate one or more variables. *weight and/or size does not include electronics and/or batteries. **B** User with amputation wearing the prosthesis. **C** ELSA rendering highlighting its main components. **D** Exploded view showing the removable battery pack and interchangeable sole.

The last couple of decades has seen the emergence of many active devices, capable of replicating the propulsive behavior of biological muscles, in an attempt to normalize the gait of people with amputation: notable devices include MIT feet [9], [10], Walk-run [11], Vanderbilt leg [12], Michigan leg [13], Open-Source Leg [14], Amp-Foot [15], CYBERLEGs feet [16], [17] and Utah leg [18], [19]. Recent devices with their respective size and mass are reported in Fig. 1A. While these devices exhibit promising mechanical capabilities, their ability to deliver significant functional improvements is not always guaranteed, as evidenced by recent studies [20], [21]. Indeed, achieving comprehensive user adoption goes beyond mechanical performance alone. In fact, factors such as safety, weight, bulkiness, energy autonomy, comfort, and aesthetics — including considerations like noise and appearance — play equally if not more significant roles in the successful adoption of these devices. Technical choices made by the aforementioned designs sometimes make it impossible to reach all these features at once.

In particular, the prosthesis size and weight are critical parameters. Whereas having a longer residual limb improves the functional outcome and energy expenditure after a transtibial amputation [22], it also restricts the prostheses that can be fitted. This issue is aggravated for patients undergoing an ankle disarticulation [23]. To accommodate users with more distal amputation, it is essential to minimize the build height of prostheses. However, many currently powered devices position their actuation unit proximally, i.e. above the artificial ankle joint. This choice occupies a significant portion of the missing lower leg, resulting in a substantial build height, often exceeding $20\,\mathrm{cm}$. Moreover, an heavy device has also been correlated with uncomfortable inertial efforts in the stump and an increased metabolic cost of walking [24], [25]. It is also essential that the device weight does not become burdensome when it cannot provide propulsion.

Additionally, whereas some authors such as [26] recently documented very low power modes, the performance of powered devices with a depleted battery pack is rarely considered. Yet, it is important to consider how these devices perform in such scenarios, as ensuring safety, comfort, and the ability to walk should ideally be maintained, even when no external power source is available. This would provide a graceful degradation of the device into a passive operating mode. Hybrid solutions that would offer both passive and active modes would have a distinct advantage in terms of reliability and robustness, ensuring that users could continue to rely on the device even in less-than-optimal conditions.

In the quest of reducing the bulkiness of powered devices, a common approach involves incorporating a compliant element within the system actuator, either in series or in parallel. This integrated spring delivers energy at high power levels during the gait cycle, effectively reducing the peak power and/or torque demands on the actuator [27]. In particular, Series Elastic Actuators (SEAs) can decrease the speed and, consequently, the power requirements on the motor side [28]. Additionally, SEAs excel at shielding the actuator from shocks at the cost of a reduced torque control bandwidth. Conversely, in the parallel configuration, the combined contributions of the spring and motor collectively generate the total joint torque, thereby potentially reducing the torque demanded from the motor itself. This allows for the selection of a lower gear ratio transmission and/or selection of a smaller motor, resulting in improved backdrivability and reduced reflected inertia, as an added benefit. We demonstrated in previous simulations [29] and early developments [30], [31] that combining a parallel spring with an actuator effectively leads to a globally energy-efficient system for an artificial ankle device. Indeed, considering overground walking, adding a passive parallel elastic element lowers the peak torque requirements of the complementary active module by 50% (Fig. 2B). We showed that this corresponds to a theoretical 18% reduction of electrical power consumption of the active side due to reduced losses in the actuator [29]. Finally, this hybrid architecture offers the ability to walk fully passively, with no propulsion, similarly to a passive prosthesis.

This article presents an innovative powered ankle-foot prosthesis that tackles the aforementioned limitations while building upon our prior research findings. This compact (foot-size) and lightweight device is designed to replicate the biomechanics of the missing ankle-foot complex. Our investigation focuses on the device's capability to faithfully reproduce the kinematics and kinetics of a healthy ankle. The device is first validated through benchtop experiments. Then, we report experimental trials involving four subjects with diverse amputation levels to assess its performance in diverse locomotion scenarios. We further explore how different control strategies can be employed to modulate the amount of energy exchanged between the device and the user. Finally, we show how several control parameters, the terrain, and the user itself, impact the device performance.

II. Device overview

The device herein described, namely ELSA (Efficient and Lightweight Spring Ankle), is a single degree of freedom powered ankle-foot prosthesis that aims at reproducing the biological behavior of the missing joint (Fig. 1C). Its most notable features are its low weight ($1.15\,\mathrm{kg}$ battery included), compactness (its volume fits within a shoe) and low profile (build height $11\,\mathrm{cm}$) while being capable of providing net mechanical energy to the user and up to $150\,\mathrm{Nm}$ of torque. Its range of motion goes from $12°$ in dorsiflexion to $20°$ in plantarflexion. It is a fully embedded actuation module with a removable battery pack and an interchangeable foot sole, down to $22\,\mathrm{cm}$ foot length (Fig. 1D). The total actuation unit length, including spring and battery pack, reaches $16\,\mathrm{cm}$. This is much smaller than the 5% percentile foot length of adult males $22.8\,\mathrm{cm}$ and females $22.5\,\mathrm{cm}$ [32], meaning that it could be used with any foot size. The hybrid architecture featuring a spring and motor in parallel offers users the choice to walk (i) actively, with propulsive energy assistance; (ii) regeneratively, potentially allowing for energy harvesting to recharge the device's battery; or (iii) completely turned off (passive).

A. Mechanical design

As shown in Fig. 1 and 2, the prosthesis is a combination of a 3D printed (Nylon, PA12) structural shell, a rigid actuation unit, a parallel spring and a rigid foot sole. The prosthesis is fitted with a standard pyramid adapter that provides anchoring to the user's pylon and socket. The plastic structural shell was validated by FEA load testing prior to the manufacturing, as detailed in the Supplementary Materials.

The design is based on the combination of a spring and actuator working in parallel. The spring stores and subsequently releases mechanical energy during the stance phase while the actuator can modulate the extra amount of energy injected in the cycle. The motor (EC22 4 poles, Maxon, Switzerland), selected based on previous simulation results [29], is mounted horizontally and transfers power to a ball screw (SP8x2.5, Ewellix, Sweden) via a timing belt-pulleys transmission providing a 3.6:1 gear ratio. Then the $2.5\,\mathrm{mm}$ pitch ball screw converts the rotary motion into a linear one. The nut is attached to a slider guided by rods on either side. This slider is then connected to a lever rotating around a fixed axis (joint axis) by means of a slotted pin joint. This converts the linear motion of the slider into a rotation of the lever and

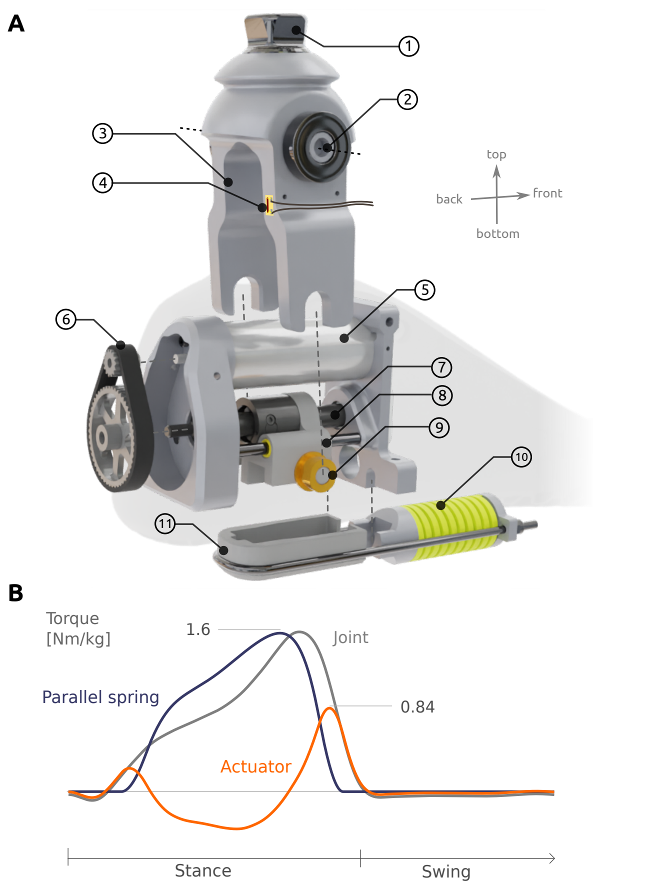

Fig. 2. **A** Exploded view of the device: (1) pyramid connection, (2) joint axle with magnet for position measurement, (3) main lever, (4) strain gauge for torque sensing, (5) motor, (6) belt-pulley transmission unit, (7) ball screw transmission, (8) slider, (9) pin joint, (10) die spring, (11) spring transmission and mechanical stop. **B** Joint torque split between the ideal spring and motor contributions, according to [29].

its pyramid connector, thus actuating the joint. The motor and gearbox can provide a peak torque of $60\,\mathrm{Nm}$ and peak speed of $36\,\mathrm{RPM}$ through a transmission with a total 456:1 gear ratio, constant over the whole angular range.

The elastic element is materialized by a steel die spring (Ressorts du Léman, Chêne-Bourg, Switzerland). Although the spring is meant to be adapted as a function of the user weight and preference, in this paper, the reference 306-406 with catalog stiffness of $199\,\mathrm{N/mm}$ was used for all users. Supplementary materials provide a detailed identification of the spring stiffness. The compliant element is unidirectional and engages with the slider during dorsiflexion thanks to a mechanical stop located at a specific joint angle ($0°$, pylon vertical). This angle is selected such that the motor, acting in parallel, does not need to work against the spring during the foot return motion (swing phase) after the powered push-off.

B. Electronics

The embedded electronics is composed of a main board that provides several functionalities: power management, actuator control and wireless communication (Fig. 3). The system is composed of a custom designed brushless motor driver (based on a STM32, STMicroelectronics, Switzerland and a DRV8302, Texas Instruments, USA) and of a general purpose dual-core microcontroller (ESP32, Espressif systems, China) with wireless capabilities. On top of this, a power management section controls the switching on and shutting down of the device. The device is fitted with an inertial measurement unit, a joint position sensor (AS5048, AMS, Premstaetten, Austria) and a custom torque sensor enabling in-situ measurement of mechanical power. This latter sensor is materialized from a single silicon strain gauge (BPY-1000-2,6-U-I-RL, BCM sensor, Belgium) affixed on the joint lever (see Fig. 2A). It forms a Wheatstone bridge with three other fixed value resistors. The output voltage of this bridge is amplified 20 times before being acquired by the microcontroller. It is only used for measurement and is not required for the device closed-loop control.

The device can be powered either using the integrated $20\,\mathrm{Wh}$ battery pack or an external power source. The latter option, which can also include an emergency stop button, connects via a dedicated connector. The internal battery pack is composed of six custom made triangular LiPo cells in series and a dedicated battery management system. This pack is not tested within this study but is expected to provide up to 5000 steps with assistance (2500 strides) which is more than the average out of home daily steps and just slightly below the total number of steps per day for transtibial amputees [33]. The pack is removable and can be replaced by a spare one. Furthermore, in a daily-life scenario, only a fraction of the steps require assistance and some steps can even recharge the battery pack, owing to the backdrivability of the transmission.

In passive mode, or when the device is shut down, the supply rail of the motor driver is isolated and connected to dissipation resistors via a normally-closed solid-state relay, as shown in Fig. 4. This setup guarantees safe walking by inducing damping via the back-electromotive force. This mode can be used for low activity ambulation, to dissipate energy when the battery is full or to allow walking when the device is off. In active operation, the relay is opened by the microcontroller (optical coupling) and the supply rail is connected to the battery.

III. Controller

A. Architecture

The control architecture is in charge of computing the motor torque in order to reproduce as accurately as possible the behavior of a sound ankle. It is composed of three hierarchical layers corresponding to those recommended in [34] and displayed in Fig. 5. Whereas the highest level detects the current locomotion task (flat-ground, stairs, etc), a mid-level controller generates gait patterns. The lowest level generates motor commands, tracking a setpoint defined by the upper level. The active torque contribution from the motor adds up to the passive parallel spring contribution.

The low-level controller outputs a motor current for the motor driver that is computed by either an impedance controller or a cascaded position controller. In impedance mode, the current is computed as the sum of a damping and stiffness contribu-

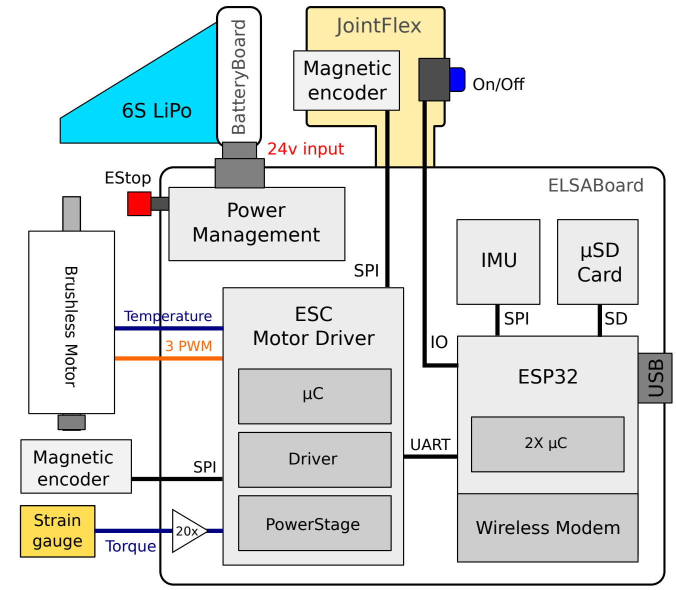

Fig. 3. ELSA electronic architecture: the main board (ELSABoard) comprises a custom motor driver, a power management unit, and a telemetry unit (ESP32). A flex PCB hosts the joint position sensor and an On-Off switch.

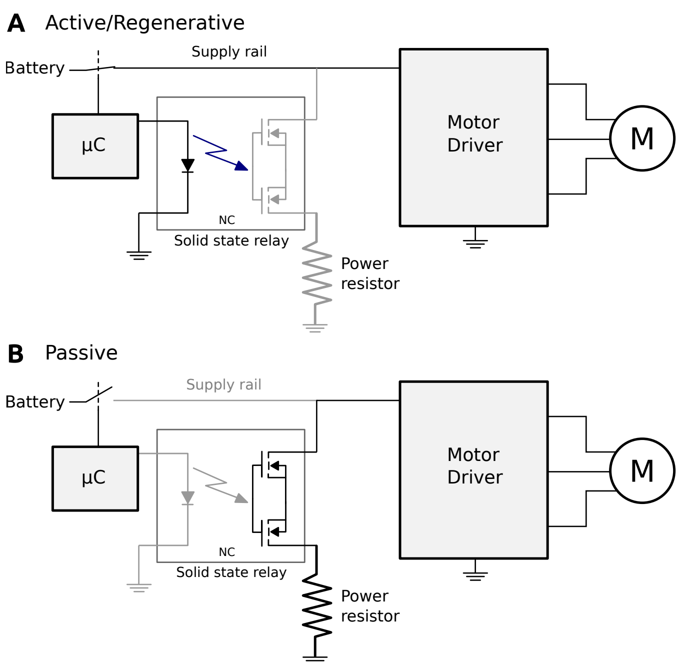

Fig. 4. Passive damping architecture (part of the power management unit): a normally-closed solid-state relay controls a power resistor that induces motor damping. The resistor is usually disconnected by the microcontroller (**A**) but connected in passive mode or when the device is switched off (**B**).

tions. Damping is controlled by two parameters, d_d and d_p, defining the damping factor in dorsiflexion and plantarflexion, respectively. Stiffness is controlled based on a neutral joint angle θ_{k_0} and virtual stiffnesses k_p and k_d for displacements with respect to θ_{k_0} in dorsiflexion or plantarflexion respectively. It is worth noting that, in dorsiflexion, this virtual stiffness comes in parallel to the mechanical one, provided by the spring. In position control, the current is the result of a cascaded position and velocity proportional-integral (PI) controllers targeting the position θ_{ref} with limited joint velocity $\dot{\theta}_{lim}$ and torque τ_{lim}. Since the torque is not directly regulated, we approximate the torque limit with a maximum motor current. The selection of the control mode and its associated parameters are determined by the upper layer. It is worth noting that, excepted for the foot return during the swing phase, the position of the joint is not enforced but is the result of interaction forces with the environment. This is obvious for the impedance controller but is also the case for the cascaded controller thanks to the implemented speed and torque saturations.

Noteworthily, the mid-level controller can either be a state machine (active mode) or a stateless controller (regenerative mode). In this latter mode, no state machine is implemented and the behavior is unchanged over the gait cycle. On the contrary, the transitions of the active mode state machine are based on kinematic rules and associated with the following low-level setpoints :

- **Stance** - Impedance control: motion damping. Transition when the joint angle reaches a dorsiflexion threshold. Within this state, the passive elastic element is also providing resistance. Optionally, the motor can modulate the passive spring stiffness by rendering a parallel virtual stiffness.
- **Push-off** - Position control: position control with target in plantarflexion. Transition when the requested joint target is reached. The torque limit is gradually increased during dorsiflexion to make the push-off action more gradual.
- **Swing** - Position control: position control with target the joint neutral position. Transition when the requested target is reached.

Notably, this controller implements no closed-loop torque control. The torque sensor is only used for device performance evaluation, i.e. mechanical output measurement. This is motivated by the fact that such sensors require an accurate calibration and drift mitigation techniques. This is feasible for short experimental sessions in the lab but challenging for a device out in the field.

The high-level controller plays a pivotal role in discerning the current ambulation task and subsequently determining the desired mid-level behavior, either active or regenerative. During the experimental session described in the present work, the appropriate task was manually selected by an experimenter through a graphical user interface on a monitoring laptop. However, a high-level controller is under development and further details can be found in [35].

B. Modes of ambulation and corresponding gait parameters

When powered on, the device can be either active or regenerative, respectively injecting propulsive energy or harvesting energy from the motion, depending on the current ambulatory activity. Indeed, activities such as standing, confined ambulation and going down a slope/ramp do not require power injection. Hence the device uses the regenerative mode. In contrast, tasks such as stairs and slope ascent or sustained overground walking do require an adequate amount of propulsive energy from the ankle [36], provided by the active mode. Fig. 5B shows the typical ankle kinematics during regenerative and

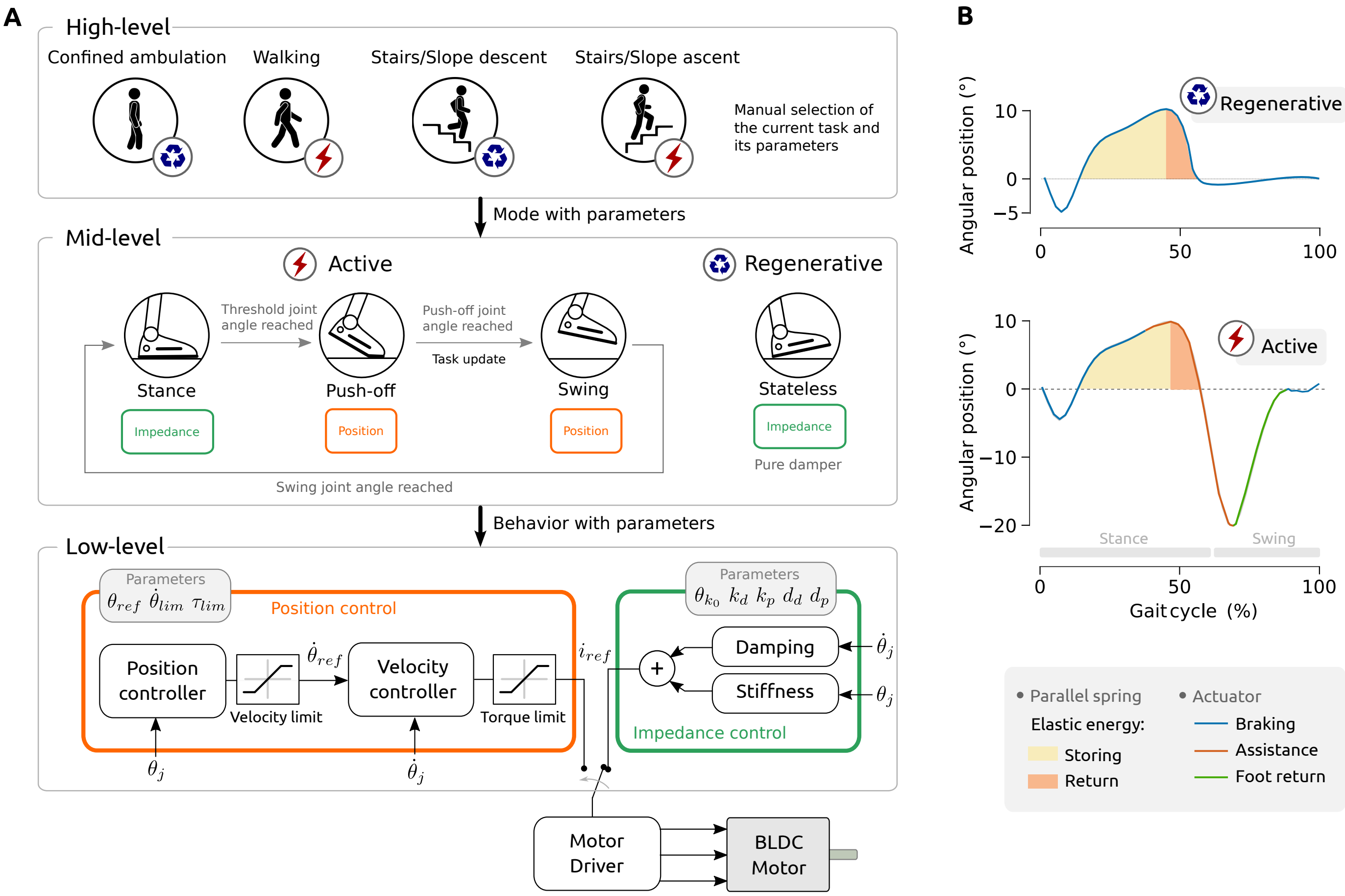

Fig. 5. **A** Controller architecture: the high level controller selects an ambulation task that defines a mode and its parameters. Depending on the mode, the mid-level controller runs either a state machine or a stateless controller, associated with behaviors. Finally the low-level controller executes the requested position or impedance behavior and outputs a current reference for the motor driver. **B** Angular trajectory of the prosthetic ankle throughout a typical gait cycle in both regenerative and active modes.

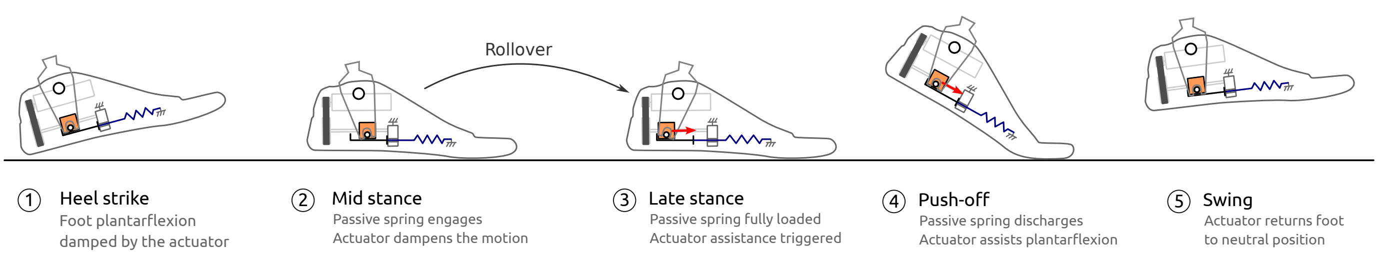

Fig. 6. Main events of a typical gait cycle in active mode: at heel strike (1), the motor damps the motion to prevent foot slap. In mid stance (2), the spring stores energy and the motor continues damping the motion. In late stance (3), a position threshold is reached and the device enters push-off (4) were both the spring and motor assist plantarflexion, effectively propelling the user forward. Finally, the foot returns to its resting position during swing (5), ready for the next step.

active modes as well as the behavior of the device at different stages of the gait cycle. The main difference between these two modes is the propulsive plantarflexion that is provided only during active push-off.

In regenerative mode, the motor brakes the motion, emulating a damper, while the mechanical spring generates supporting torque starting from mid-stance. At the end of the stance phase, the foot returns to the neutral position by harvesting the elastic energy stored in the spring. The damping amount is adjusted to produce a critically damped response in combination with the spring. This ensures that the foot returns to the neutral position without extending further in plantarflexion. Consequently, no active return motion is required during the swing phase in regenerative mode.

In active mode, as depicted in Fig. 6, the device emulates the ankle biomechanics by displaying a different behavior across three consecutive gait phases, i.e. stance, push-off, and swing. During stance, the motor damps the motion. When a threshold joint angle is reached, the device goes into the push-off phase and the motor helps plantarflexing the foot with a desired assistive torque. The physical spring discharges at the same time, effectively propelling the user. Finally, during the swing phase, the motor brings the foot back to its neutral position, in preparation for the next step. Additionally, through the adjustment of a single parameter k_d within the active mode, an active stiffness feature can be enabled. The motor assists ankle rollover by acting like a virtual spring with a negative stiffness, lowering the total joint stiffness. This virtual spring, with a lower stiffness relative to the physical spring, thus actively injects energy into the latter.

For both modes, i.e. active or regenerative, the prosthesis mid-level controller has been designed in such a way that some of its key parameters should be personalized as a function of individual preferences. In regenerative mode, only two parameters are tuned, the damping in dorsiflexion and plantarflexion, i.e. d_d and d_p. When the prosthesis operates in active mode, six parameters can be tuned: the dampings d_d and d_p, θ_{trig} the trigger angle where the assistance starts to be provided, τ_{lim} the target level of assistance, θ_{tar} the target angle during push-off, and k_d the negative stiffness in dorsiflexion to actively compensate the parallel spring. It is important to note that the parameter k_p is not utilized in regenerative and active modes. However, future iterations will leverage this parameter in modes that necessitate a stiffness effect during plantarflexion. Typically, it could be used during standing to generate torque that prevents plantarflexion, thereby enhancing stability.

Additionally, the device can be used powered-off (passive), in which case the motor is passively braking joint motion, similarly to the regenerative mode, while the parallel spring still provides the baseline torque profile, thus emulating a spring-damper behavior. The embedded electronics is designed such that any regenerative energy is dissipated in power resistances that automatically connect when the device is turned off, and are disconnected otherwise (see Fig. 4). This later mode allows an infinite walking time even with no battery connected. The amount of damping is controlled by the dissipation resistor and can be adjusted to exhibit a critically damped response in combination with the spring.

IV. Preliminary bench-top validations

The prosthesis was first validated on a test bench capable of replicating the ankle motion (see [31], [37] and Supplementary Materials for details about the system). This allowed the actuator performance to be evaluated prior to walking with the device.

A. Backdrivability and reflected inertia

The backdrivability and reflected inertia are important characteristics of the device performance. A high backdrivability and low reflected inertia are required to generate accurate torque without a closed-loop torque control. In order to quantify these characteristics, the test bench was requested to apply a sine trajectory to the joint with an amplitude of $14°$. The motor from the prosthesis was electrically disconnected but mechanically coupled. The resulting torque was measured for different frequencies. A system identification procedure was performed in the time-domain, minimizing the error between the recorded data and a model taking into account static friction, viscous friction and reflected inertia, captured by the following equation:

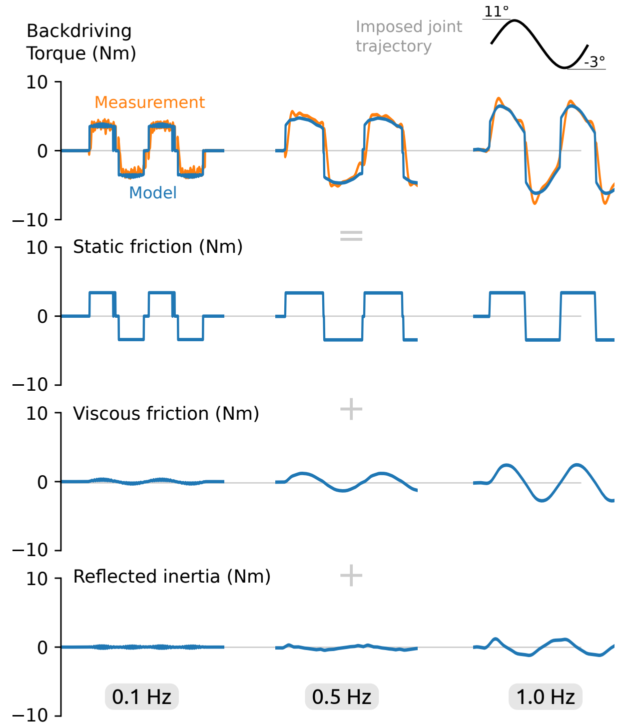

Fig. 7. System identification of the static friction, viscous friction and reflected inertia seen at the joint. The prosthesis was driven to follow a sinusoidal trajectory while the reaction torque was measured.

$$\tau = f_s \text{sign}(\dot{\theta}) + f_v\dot{\theta} + I\ddot{\theta}$$

where θ is the joint position, τ is the backdriving torque, f_s is the static friction coefficient, f_v the viscous friction and I the reflected inertia. The best-fit parameters are identified to be $f_s = 3.4\,\text{Nm}$, $f_v = 3.2\,\text{Nm/rad/s}$, $I = 0.226\,\text{kgm}^2$. The quality of this fit and respective contributions at different frequencies are shown in Fig. 7.

These low values in comparison to the total torque generated by the device to propel the user suggest a good backdrivability and low reflected inertia. In particular, the identified inertia is in agreement with the value calculated from the CAD (equal to $0.21\,\text{kgm}^2$).

B. Torque generation and measurement

In order to evaluate the actuator torque capabilities and torque measurement ability, a benchtop experiment was conducted with the physical spring removed. The test bench was instructed to drive the joint following a typical flat-ground walking trajectory, although at a slower speed ($0.2\,\text{Hz}$) due to test bench limitations. The internal controller was requested to follow the state machine shown above while the resulting joint torque was measured both by the test bench and by the internal torque sensor. The results from Fig. 8 suggest a good correlation between both signals and the ability to generate active push-off torque up to $60\,\text{Nm}$.

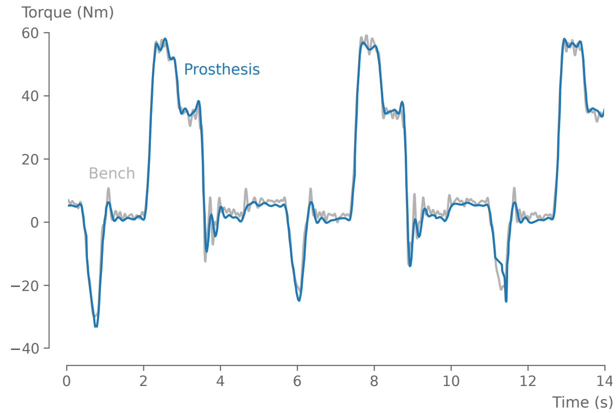

Fig. 8. Torque measurement on the test bench during several typical walking cycles. Both torque measurements (from the bench and the internal sensor of the prosthesis) overlap, suggesting a good measurement quality provided by the internal sensor.

C. Noise evaluation

Supplementary Materials include videos demonstrating the experiments conducted with the four users with amputation, which assess the noise level produced by the device during walking. In parallel, a short experiment was independently conducted in order to provide a more quantitative assessment. A non-amputee individual wore the prosthesis using a custom-made adapter. The individual was instructed to walk with the prosthesis operating in active mode, while an operator was placed at a fixed distance of 1 meter from the walking path. The experiment took place in a quiet laboratory environment, free from external noise interference. Measurements were taken as the user passed in front of the operator, using a sound level meter (CENTER 320, Center Technology Corporation, Taiwan) with a range of 30 dB to 130 dB. The experiment was repeated 3 times. The recorded noise peaks ranged between 60-65 dB, which is slightly above the sound produced by typical household appliances, i.e. around 50 to 60 dB [38].

V. Experimental methods with prosthesis users

A. Participants

Four participants – two transtibial (TT) and two transfermoral (TF) amputees – were recruited for this study, with the following characteristics (mean $\pm$ std): age 50 ± 7 years, body weight 83 ± 16 kg, and height 1.77 ± 0.10 m (Table I). Inclusion criteria comprised unilateral amputation, weight ≤ 110 kg, build height ≥ 11 cm, and K-level (Medicare Functional Classification Level) $\geq$ K3. All participants had prior experience in regularly testing new prototypes and were considered experienced in using prosthetic devices. Participants S1, S2, and S3 were testing the prototype for the first time, while participant S4 had approximately 4 hours of prior experience with it in the year preceding this session. The study procedure received approval from the Icelandic National Bioethics Committee, and all participants signed an informed consent form before the first acquisition.

TABLE I
Participant demographics.

ID	Age (years)	Sex	Body mass (kg)	Height (m)	Level	Prostheses
S1	47	M	90	1.82	TF	Proprio Foot Rheo Knee
S2	57	F	65	1.59	TT	Pro-Flex LP
S3	39	M	71	1.86	TF	Pro-Flex Pivot Rheo Knee
S4	55	M	106	1.79	TT	Pro-Flex Pivot

B. Protocol

The experimental sessions were conducted in the motion lab located within the premises of Össur company (Reykjavik, Iceland). The lab is equipped with a treadmill (Scheinworks, Germany), an 8-meter long walkway with an adjustable slope, and a 12-step staircase equipped with a safety ramp. The entire experimental protocol spanned approximately 4 hours and took place within a single day. Initially, the ELSA prosthesis was aligned by a Certified Prosthetist/Orthotist (CPO) while the user was wearing their daily shoes. To fine-tune the alignment, participants executed a few unpowered steps. Subsequently, the prosthesis was powered on, allowing for any necessary adjustments to be made.

Next, the device parameters were tuned. Plantarflexion damping d_p was carefully adjusted to ensure consistent and stable movement after initiating ground contact, while avoiding undesired foot slap. Regarding dorsiflexion damping d_d, the minimum value required to prevent oscillations in the angular speed trajectory was first tested. The damping level was increased only if the user preferred receiving more braking. In addition, the trigger angle θ_{trig} was tuned to provide users with more forward propulsion than upward push. As observed in prior pilot experiments, it was noted that a higher value of this angle resulted in greater mechanical energy being provided to the user. The target angle in plantarflexion during push-off θ_{tar} was adjusted to ensure user comfort while walking. In cases where the user had concerns about stumbling, the angle was reduced, which resulted in a faster foot return during swing. Finally, the assistance level τ_{lim} was initially set at a low value, i.e. 30 Nm, gradually increased as the user acclimated to the assistance. Once all the parameters were properly configured, participants were encouraged to walk around the testing area to familiarize themselves with the functionality and behavior of the powered prosthesis.

Following fitting and tuning (approximately 30 minutes), users were asked to walk on the treadmill and to define their preferred walking speed (self-selected speed). Afterwards, the recorded session could start. For each experiment, internal real-time data of the prosthesis were recorded for approximately 20 seconds once a stationary state was reached. The treadmill session consisted of two parts: walking with the prosthesis in active and regenerative modes at self-selected speed, followed by walking in active mode with various parameter variations, including assistance level, trigger angle, active stiffness, and walking speed. Participants were then instructed to ascend the 12% fixed slope ramp in active mode and descend it in regenerative mode. The final task consisted in ascending and descending the stairs. The number of recorded cycles during the ramp and stairs tasks was lower as compared to treadmill walking, although we ensured that a minimum of three successive prosthetic steps were consistently recorded.

C. Data processing and analysis

Real-time telemetry data were wirelessly acquired from the prosthesis to a monitoring laptop via Bluetooth (details about the setup are available in the Supplementary Materials). Subsequently, the data were processed and analyzed in post-processing. Time-dependent data were received from the prosthesis and then normalized over gait cycles. The starting point of the cycle was defined by the initiation of the plantarflexion movement during heel strike. Phase-dependent averages and standard deviations were computed for each signal. Based on these collected data, both mechanical and electrical energy could be calculated.

Mechanical energy: Computing mechanical energy E_m (J) going through the prosthesis joint, involved integrating the corresponding mechanical power P_m (W) over time. It can also be expressed as the integral of the area under the curve of torque versus angular position, i.e.:

$$E_m = \int P_m(t)\ dt = \int -\tau(t)\ \dot{q}(t)\ dt = -\int \tau(q)\ dq \quad (1)$$

with τ (Nm) the torque provided by the prosthesis to the user and $\dot{q}$ (deg/sec) the angular speed. In this study, the sign of the energy was determined from the user's perspective, i.e. with positive energy representing energy delivered by the prosthesis to the user, and negative energy indicating energy harvested from the user. The negative sign in Equation (1) derives from this convention used for sign of the joint torque. To calculate the cumulative mechanical energy, energy was computed at each sample of the gait cycle and then summed with the previously accumulated total value. This approach allowed for a comprehensive analysis of the overall mechanical energy dynamics throughout the gait cycle, providing valuable insights into energy transfer.

Electrical energy: The electrical energy going through the prosthesis battery provided quantification of the energy consumption and efficiency of the prosthesis. This electrical energy E_e (J) was computed by integrating the electrical power P_e (W) over time, i.e. as the integral of the product of the battery voltage u_{bat} (V) and the current flowing out of the battery i_{bat} (A):

$$E_e = \int P_e(t)\ dt = \int u_{bat}(t)\ i_{bat}(t)\ dt \quad (2)$$

However, the total current going through the battery i_{bat} was not directly measurable by the prosthesis. Therefore, it was estimated from the motor current thanks to a model detailed in the Supplementary Materials.

VI. Results with prosthesis users

The prosthesis was validated with users with amputation across different experiments.

Fig. 9. Photographs of the four participants performing various ambulation tasks while wearing the prosthesis: S1 (TF) climbing a ramp in active mode, S2 (TT) descending stairs in regenerative mode, S3 (TF) walking on a treadmill in active mode, and S4 (TT) climbing stairs in active mode.

A. Tuning of the prosthesis parameters

The trigger angle was generally set at $\theta_{trig} \simeq 10°$ for all users, except for S2, who opted for an earlier value of approximately $7°$. Since they were the lightest user and used the same spring as the other ones, user S2 faced challenges in achieving high angles in dorsiflexion during the stance phase. Additionally, participants S3 and S4 had their target push-off angle θ_{tar} reduced to respectively $-10.5°$ and $-10.3°$ in order to mitigate their fear of stumbling, whereas S1 and S2 maintained a target angle of approximately $-15°$. Users S2 and S3 expressed a preference for a lower damping level in plantarflexion d_p, while users S2, S3, and S4 requested a higher damping level in dorsiflexion d_d. The preferred level of assistance for all users was consistently set to the maximum value of $\tau_{lim} = 50\,\mathrm{Nm}$. It is worth noting that users with transfemoral (TF) amputations tended to choose a slower walking speed on the treadmill, i.e. $0.97\,\mathrm{m/s}$, compared to the higher speeds of $1.11\,\mathrm{m/s}$ and $1.28\,\mathrm{m/s}$ selected by users with transtibial (TT) amputations. A more detailed overview of all parameters selected by the four users in each ambulation task can be found in the Supplementary Materials.

B. Validation with treadmill walking

Fig. 9 shows the subjects participating to the different ambulatory activities, with their corresponding control modes. Fig. 10A highlights the kinematic and kinetic trajectories for user S1 while walking on the treadmill with ELSA in both regenerative and active modes. As reference, benchmark trajectories from a non-amputee individual are included as well [39]. Throughout the majority of the stance phase (foot rollover), the prosthesis in both modes closely replicates the trajectory of a biological ankle. However, a clear bifurcation arises during the push-off phase: in the regenerative mode, the prosthesis exhibits a direct return to its initial position, devoid of active propulsion. In contrast, the active mode mirrors a biologically-relevant plantarflexion, similarly to a sound ankle. The prosthesis in both modes reproduces the torque trajectory of a biological ankle, although the push-off torque peaks at $1.4\,\mathrm{Nm/kg}$, i.e. about 12% lower than a sound ankle. Plotting the torque vs. angular position curve further highlights the difference between both modes. During early stance, when the dorsiflexion angle and ankle torque rise in parallel, both curves overlap. Subsequently, thanks to the assistance provided, the curve of the active mode displays a counterclockwise pathway, capturing the fact that energy is injected by the device. Conversely, the regenerative mode curve follows a clockwise path, indicative of a reduction in overall energy, as it is harvested by the prosthesis. By comparing the trajectory obtained when the prosthesis is in active mode with the reference one, it appears that the surface area under the curve is smaller in the former than in the latter. This captures that the prosthesis injects less mechanical energy than a biological ankle during healthy walking, i.e. about 0.076 J/kg vs. 0.23 J/kg in this case. In terms of mechanical power, the peak values reached during push-off are equal to $35\,\mathrm{W}$ when operating in regenerative mode and $141\,\mathrm{W}$ in active mode, which represents an increase of $300\,\%$. When compared to a biological ankle, which has a peak power output of $3.6\,\mathrm{W/kg}$ or $324\,\mathrm{W}$ for a 90kg person (S1), these values correspond to $11\,\%$ and $43\,\%$, respectively.

To provide a comprehensive overview of the gait patterns observed with the four users, Fig. 10B illustrates the kinematic and kinetic trajectories during level ground walking in active mode. For all users, the torque vs. angular position curve exhibits a counterclockwise pattern, indicating that the prosthesis provides net positive energy. This confirms the fundamental capability of the active prosthesis to deliver mechanical energy during steady-state walking. Moreover, the kinematic and kinetic curves align across cycles with small variability, indicating that the users maintain a consistent walking pattern.

In the following paragraph, we discuss with more details the inter-individual differences visible on these curves, and how they relate to parameters of the prosthesis controller. Range of motion during early stance is higher for users S2 and S3, reaching a maximal plantarflexion angle of $(-6.2\pm0.7)°$ and $(-8.4\pm0.5)°$, respectively. The heel strike damping parameter governing plantarflexion d_p is set to a lower value for these two users compared to participants S1 and S4, as reported in Section VI-A. Consequently, the plantarflexion movement is less restrained, resulting in a larger motion. During the stance phase, the dorsiflexion movement reaches a maximal angle of $\sim10°$ for users S1, S3, and S4, while S2 reaches a slightly lower value of $\sim8°$. This disparity is likely attributed to user S2 having the lightest body weight, while the prosthesis was equipped with the same spring for all users during this session. Consequently, user S2 is able to compress the spring less as compared to the others and the push-off trigger angle is set earlier. For participants S3 and S4, the target angle for plantarflexion during push-off was set to $\theta_{tar} \simeq -10°$, as opposed to $-15°$ for users S1 and S2, see Section VI-A. Analyzing the torque versus angular position curves reveals however that users S1 and S2 do not gain any further advantage from assistance beyond $-10°$. Indeed, the torque is equal to zero beyond this angle, indicating that their foot is no longer in contact with the ground. This suggests that the target angle for plantarflexion could have also been reduced for these users. Furthermore, both lightest users, namely S2 and S3, achieve a higher peak torque when normalized to their weight, with a value of $1.7\,\mathrm{Nm/kg}$, in contrast to approximately $1.4\,\mathrm{Nm/kg}$ for participants S1 and S4. This observation suggests that the torque provided by the device for heavier users could be improved, by increasing either the stiffness of the spring or the assistance provided by the motor.

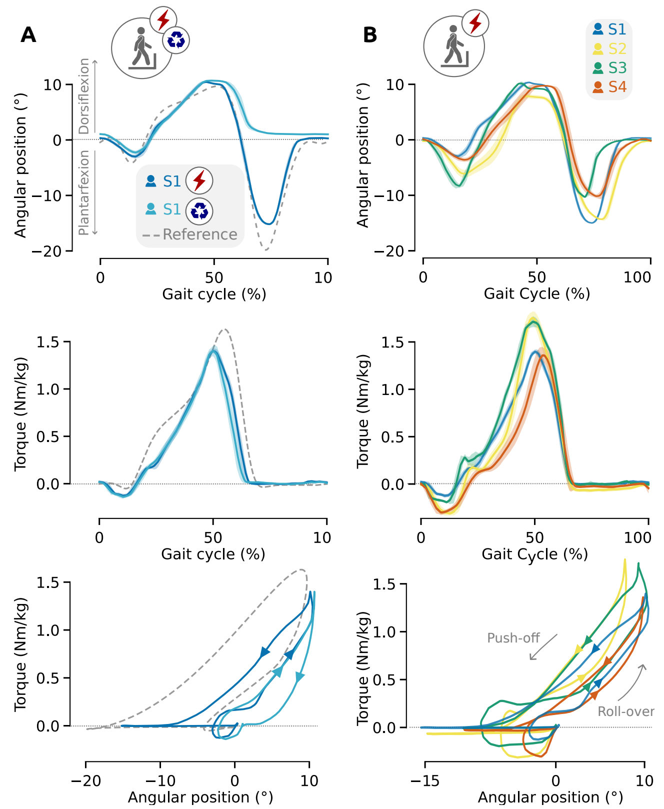

Fig. 10. **A** Angular position, torque and mechanical power (mean ± std) throughout a gait cycle, and torque vs. angular position (bottom) trajectory (mean only), during treadmill walking at a comfortable speed. Comparison is made between both main control modes, i.e. regenerative and active, for participant S1 (TF). The light-grey dotted lines represent reference trajectories obtained from users without amputation, adapted from [39]. **B** Equivalent trajectories are displayed for all four users, with the prosthesis operating in active mode.

C. Validation across various ambulation tasks

Subsequently, participants proceeded to test the device under different ambulatory modes, specifically ramp and stairs ascending/descending. In this section, we highlight individual results obtained with representative participants, and we mention discrepancies observed with others when relevant. Fig. 11 displays the angular position and torque of the ankle joint for the representative subject S4 over a mean gait cycle for four distinct ambulation tasks, namely ramp and stairs ascending/descending. It should be noted that the reference trajectories for ramp ascending and descending [40] were recorded with non-amputated participants on a steeper slope than the one used in our study, i.e. 15% compared to 12%.

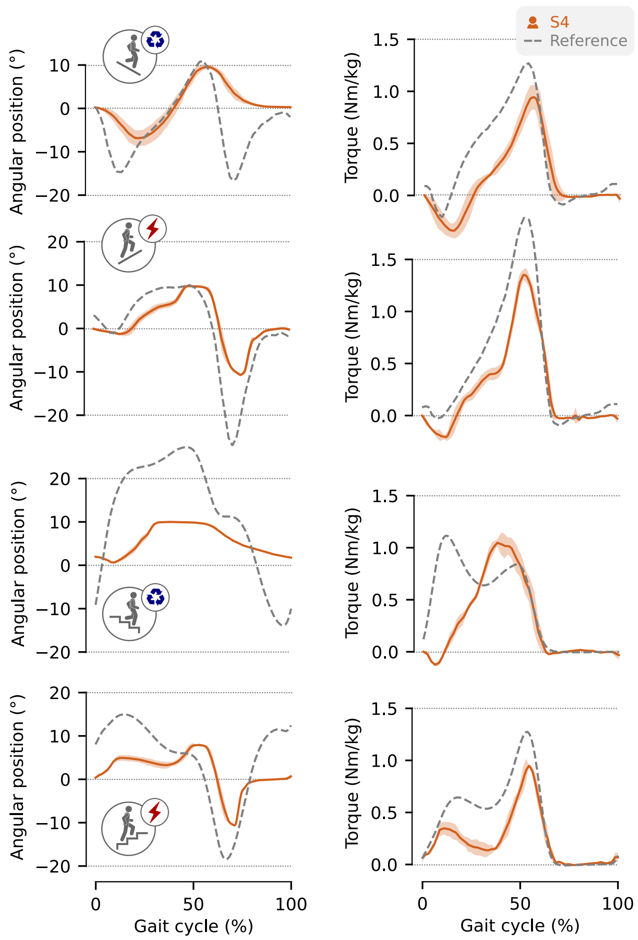

Fig. 11. Angular position and torque (mean ± std) over a gait cycle during stairs/slope ascending and descending. The prosthesis operates in regenerative mode for descending and active mode for ascending. Experimental results are presented for a representative participant, S4 (TT). Reference trajectories from users without amputation are depicted as light-grey dotted lines, adapted from [40], [41].

When descending a ramp, the prosthesis operates in regenerative mode. Participant S4 expressed a preference for more support specifically in dorsiflexion, which translates into more damping. As a result, the corresponding parameter was doubled compared to walking on level ground. The reference curve of the angular position exhibits a pronounced plantarflexion during early stance, reaching a maximum angle of $-14.6°$. In contrast, our experimental data recorded an average angle of $(-7.6 \pm 0.8)°$. Notably, no negative position peak in plantarflexion is observed during the push-off phase, which is consistent with the selected gait mode, i.e. regenerative, where no powered push-off is happening. This deviates however from normative data. Furthermore, the torque trajectory closely follows the biomechanical reference, albeit with a delayed peak torque of $(1.0 \pm 0.1)\,\mathrm{Nm/kg}$, approximately 23% smaller than the one of a sound ankle.

During ramp ascent, the prosthesis operates in active mode using the same trigger angle as in level ground walking. The reference curve exhibits a plateau in dorsiflexion during the stance phase. However, for user S4, this pattern is only noticeable in late stance, when the prosthesis reaches its maximum range of motion. The peak torque observed is $(1.4 \pm 0.1)\,\mathrm{Nm/kg}$, which is approximately 26% lower than the reference peak torque.

Similarly as for slopes, the prosthesis functions in regenerative mode during stair descent and in active mode during stair ascent. In the case of user S4, the prosthetic ankle achieves a dorsiflexion angle of $10.0°$, limited by the device's range of motion, which is notably lower than the reference peak of $27.3°$. Regarding kinetics, the participant produces a single peak torque, while the reference data suggests a double peak. It is important to note that people with amputation often adopt a different gait pattern during stair ascent and descent due to the limitations of their passive daily-life prostheses. Consequently, due to the lack of an extended familiarization period with the prosthesis, care should be taken when comparing these data with the reference trajectories [41]. For instance, users with amputation, particularly those with transfemoral amputation, face difficulties when attempting to fully place their entire foot onto a step during the descent of a staircase. Instead, it is common for these individuals to position the midfoot at the edge of the step, using it as the center of rotation of their leg while maintaining limited dorsiflexion in the ankle. This is the reason why no data was collected with User S3. However, the representative user (S4) had no difficulty placing the whole ELSA prosthetic foot on the step during descent. For user S1, benefiting from the prosthesis assistance during stairs ascent proved challenging. Despite lowering the activation threshold, this user could not perform sufficient dorsiflexion movement to trigger the active push-off. In the case of participant S4, the trigger angle was reduced to $8°$, representing an 18% reduction compared to the angle set during level ground walking. Furthermore, analysis of the angular trajectory reveals that the biological ankle exhibits a slight dorsiflexed angle as it approaches the step. Whereas this toe lift feature has not yet been incorporated into the control system of ELSA, it holds potential for further investigations. Finally comparing the torque profile of user S4 with the reference curve reveals the existence of two local peaks, although of smaller amplitude as compared to the reference values.

D. Analysis of energy flows

Fig. 12 reports the energy-related results derived from both modes across a range of ambulation tasks for the four users. The signs of the computed net mechanical energies align with expected results. Indeed, the regenerative mode proves to have a negative energy balance, as indicated by the negative sign. In contrast, the active mode yields positive mechanical energy, demonstrating the potential of the prosthesis to provide assistance to the user.

In regenerative mode, a greater amount of mechanical energy is recovered during ramp descent compared to level ground walking. This is due to the larger damping coefficients used in the controller and the more pronounced plantarflexion movement in early stance during ramp descent. On the other hand, participants experienced a significant increase in mechanical energy (average of 194%) during ramp ascent as compared to level ground walking. This can be attributed to

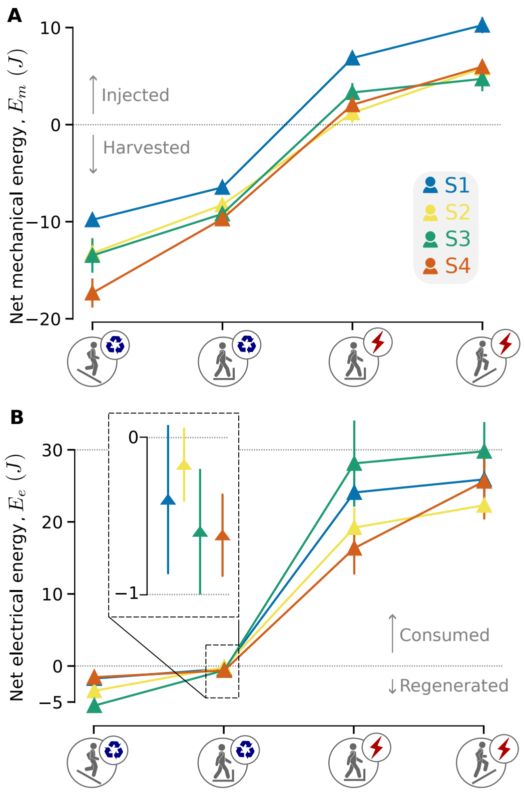

Fig. 12. **A** Net mechanical energy E_m (mean $\pm$ std) computed over a gait cycle for various ambulation tasks, including ramp descent, level ground walking and ramp ascent, for each participant. The prosthesis operates in regenerative mode for the first two tasks and in active mode for the later ones. **B** Net electrical energy E_e (mean $\pm$ std) over a gait cycle consumed by the motor, for the same conditions.

two factors observed during ramp ascent: first, participants keep their prosthetic foot in plantarflexion for a longer duration during late stance, and second, lower amplitudes in plantarflexion are reached during early stance, resulting in reduced angular speeds of the joint. Consequently, less energy is harvested by motor-induced damping during this movement. During level ground walking in active mode, participant S1 benefits from the highest amount of energy from the assistance provided by the prosthesis. The mean mechanical energy E_m computed over a complete gait cycle, is at least two times greater than for the other three participants, i.e. (6.9 ± 0.7) J vs. 1–3 J. Notably, user S1 experienced the highest level of assistance, reaching (10.2 ± 0.8) J of mechanical energy during ramp ascent. In sum, our controller can generate different energetic outcomes due to the different kinematics and the adaptation of a few parameters.

Electrical energy balances are pictured in Fig. 12B. In the regenerative mode, a negative value of electrical energy indicates the potential for energy harvesting to recharge the battery. Participant S3 reaches $E_e \simeq -6$ J while descending a ramp, meaning that the battery is effectively recharging. During level ground walking, E_e is between -0.2 J and -0.6 J. This implies that the consumption of the device is more than fully compensated by the harvested energy. Consequently, the prosthesis can operate indefinitely in this mode without consuming extra electrical energy from the battery. While walking on level ground in active mode, the electrical consumption ranges from 15 J to 30 J. A first step towards explaining the difference across users is to analyze the walking speed, and therefore stride duration. Participant S3 has a stride duration of 1.6 s, S1 of 1.3 s, while S2 and S4 of about 1.1 s. This highlights a trend showing that the longer the stride duration, the higher the power consumption. Indeed, the longer the prosthesis is in contact with the ground, the longer the assistance is provided, resulting in an increase of power consumption. Finally, during ramp ascent in active mode, the consumption for each user increases as compared to level ground walking.

We observe that there is no clear relationship between mechanical and electrical energy across participants and ambulation modes. In other words, the energy efficiency of the device is not constant. Several factors can explain this observation. Firstly, the net electrical energy over a gait cycle increases when the user walks at a slower pace due to continuous electronics consumption, which remains unchanged regardless of walking speed. Additionally, each user's gait style influences their energy production and consumption patterns, since the different elements of the prosthesis are engaged in varying ways. For example, a user may compress the spring more or enjoy greater benefit from the assistance by keeping their prosthetic foot on the ground for a longer duration. Differences in gait may also correspond to variations in amplitudes reached during early stance, resulting in higher speeds and increased braking forces.

E. Sensitivity analysis of control and gait parameters

Fig. 13 investigates the impact of control and gait parameters, namely the trigger angle, assistance level, and walking speed, on the gait dynamics. The prosthesis operates in active mode for the three selected experiments. Each subfigure displays two plots: one illustrating torque vs. angular position and the other depicting the cumulative mechanical energy over a complete gait cycle. This visual representation, which gradually captures the accumulation of mechanical energy throughout the cycle, offers valuable insights into distinct energy phases. Initially, the energy storing phase corresponds to negative mechanical power during the loading phase of the parallel spring. Subsequently, the cumulative energy shows a positive increase due to the positive power provided by the actuator during the push-off phase.

Fig. 13A highlights the sensitivity of the gait pattern as a function of the trigger angle θ_{trig}. Increasing the angle from 8.0° to 10.3° results in a substantial rise in cumulative mechanical energy from (0.025 ± 0.010) J/kg to (0.046 ± 0.011) J/kg, or from 1.78 J to 3.27 J, representing an increase of 84%. Moving the trigger angle to an earlier position causes the prosthesis to start the plantarflexion movement earlier, resulting in a lower maximum angle reached in dorsiflexion. As a consequence, the parallel spring experiences less compression, leading to a lower negative peak in cumulative mechanical energy. Regarding the increase in cumulative mechanical energy in the later part of the cycle, there is a larger difference between the negative peak and the final plateau when using

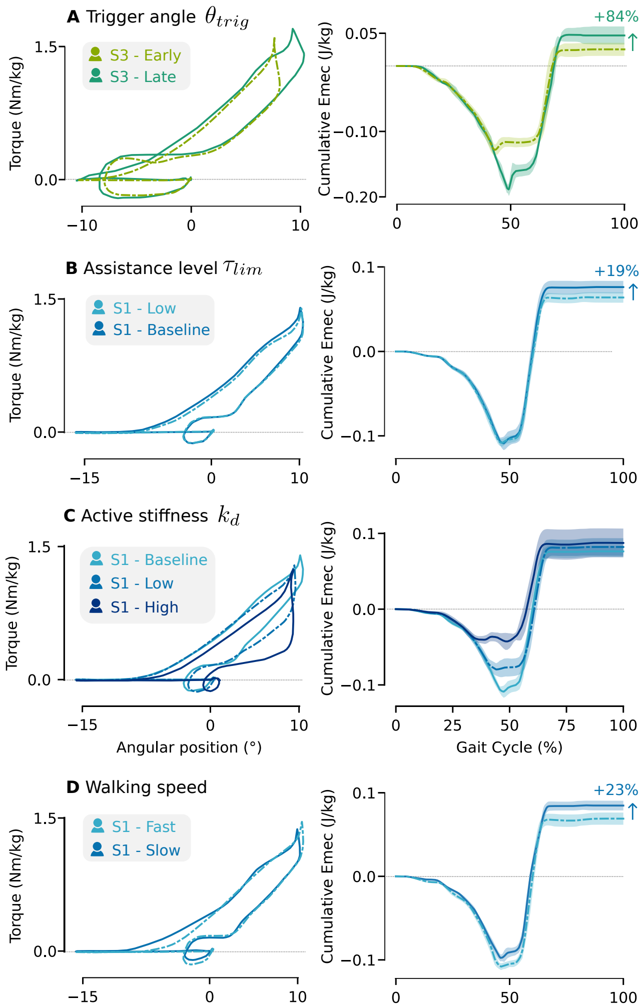

Fig. 13. Tuning of prosthesis parameters (trigger angle, stiffness and assistance level) and gait parameter (walking speed). The torque vs. angular position (mean only) and cumulative mechanical energy (mean $\pm$ std) over a gait cycle are depicted. **A** The trigger angle θ_{trig} is the angular position in dorsiflexion at which assistance is initiated. Results are shown for participant S3 (TF). **B** The assistance level τ_{lim} indicates the actuator contribution during the push-off phase. Results are presented for participant S1 (TF) with low and baseline assistance levels, specifically $40\,\mathrm{Nm}$ and $50\,\mathrm{Nm}$. **C** Active stiffness feature k_d is evaluated with three levels: baseline, low and high, respectively with k_d equal to 0, 3.49 and $6.98\,\mathrm{Nm/deg}$. Results are shown for participant S1 (TF). **D** User S1 data are provided walking at both slow and fast speeds, namely $0.83\,\mathrm{m/s}$ and $1.11\,\mathrm{m/s}$.

a late trigger angle. This difference is likely due to a longer traveled distance during the stance phase. This increases the mechanical energy provided due to the motor having more time to deliver assistance. Based on these findings, it is recommended to consider the latest possible trigger angle during the tuning phase. In Fig. 13B, the low and baseline assistance levels correspond to an actuator contribution of $40\,\mathrm{Nm}$ and $50\,\mathrm{Nm}$, respectively. Increasing the assistance level has a positive impact, resulting in a 19% increase in cumulative mechanical energy. These two first experiments highlight the importance of the tuning phase for optimal utilization of the prosthesis. Careful adjustment of the parameters is essential to fully leverage the provided assistance.

Fig. 13C shows the effect of partially compensating the physical spring with a virtual spring emulated by the motor. This means that the motor helps the user in compressing the physical spring. It highlights that the rendered stiffness of the joint is indeed lower during the spring compression phase. The slope of the early stance curve is lower as the compensation level is higher, resulting in a lower stiffness felt by the the user. When the motor stops compensating for the spring, the stored energy within the spring is released, corresponding to sharp torque increase. Concurrently, the motor begins to inject energy for push-off. We can observe that the dorsiflexion angle achieved is reduced when active stiffness feature is applied. This suggests that the transition between the stiffness modulation and the push-off injection is too abrupt. Therefore, it disrupts a smooth angular progression of the user's joint. In terms of cumulative mechanical energy, a higher k_d corresponds to a lower negative peak, since the user expends less energy to compress the spring.

Next, the device performance is evaluated across two different walking speeds. As depicted in Fig. 13D, when walking at a slower pace, users derive greater advantages from the prosthesis assistance. By reducing the walking speed from $1.11\,\mathrm{m/s}$ to $0.83\,\mathrm{m/s}$, the cumulative mechanical energy increases by 23%. Indeed, the extended contact of the user's foot with the ground during the plantarflexion phase allows the prosthesis to deliver assistance for a longer duration.

VII. Discussion

Developing a powered ankle-foot prosthesis that faithfully replicates the biomechanics of the missing limb is a challenging undertaking, primarily due to the substantial peak torque and power demands, even during normal-speed locomotion. The added complexity arises from the concurrent need to achieve a lightweight, compact, and high-performance design. By developing ELSA, we tried to address those challenges.

In this work, we achieved to develop a foot-size, low profile ($11\,\mathrm{cm}$) and lightweight ($1.15\,\mathrm{kg}$) powered prosthesis reproducing ankle dynamics. This device provides users with multiple walking modes: active walking with propulsive energy assistance, regenerative that enables energy harvesting to recharge the battery, and passive where the device is turned off. Key parameters such as the trigger angle, damping levels, and assistance level can be tuned to personalize the prosthesis behavior to each user. Starting with a default profile and following clear parameter guidelines (as outlined in Section V-B), the customization process takes approximately 15 minutes. Furthermore, the actuator is able to adjust the rendered joint stiffness through the active stiffness feature, while having a single physical spring.

The prototype was validated through an experimental session with four users with varying levels of amputation. The recorded data indicate that both the kinematic and kinetic profiles closely resembled those of non-amputee references. Our device was capable of transmitting approximately $7\,\mathrm{J}$ of mechanical energy to the user during level ground walking. This increased to about $10\,\mathrm{J}$ during ramp ascent. The device could provide peak torques up to $150\,\mathrm{Nm}$. In regenerative mode, our results show a net negative energy during flat ground walking, thus unlocking the potential for continuous operation without the need for external recharging. This is in contrast to a similar feature described in [42] which could not reach a negative energy.

While having a longer residual limb enhances socket stability, it can limit compatibility with existing devices. Our design addresses this challenge by offering compactness and a low profile, making it a good fit for users with a very low amputation level. Additionally, its discreet form factor allows it to seamlessly fit within a standard shoe. Authors do not always disclose precise build height and weight measurements, but to the best of our knowledge, there is no fully embedded device reaching such a low weight and build height as ours (see Fig. 1A).

We believe we achieved these results thanks to several design choices. As demonstrated in earlier works [29], placing a parallel spring into the design lowered the torque demands from the motor, enabling the selection of a lower gear ratio. This not only positively impacted efficiency and power consumption but also led to a reduction in reflected inertia. Indeed, given that the inertial load at the joint is dependent on the square of the gear ratio, halving the motor peak torque translated to a fourfold decrease in reflected inertia. This, in turn, allowed us to opt for a small, lightweight, and low-inertia motor ($22\,\mathrm{mm}$, $170\,\mathrm{g}$), further enhancing backdrivability and overall integration. This high backdrivability and low reflected inertia remove the need for a shock absorption mechanism at heel strike. Instead, the device naturally performs a plantarflexion movement governed by a damping model, closely emulating the behavior of the human ankle.

The integration of a passive spring, combined with a backdrivable actuator, enables the prosthesis to function in a fully passive mode, resembling a spring-damper configuration. The spring generates movement resistance from the neutral position, i.e. 0°, while walking. This passive mode proves useful in scenarios involving depleted batteries or technical failures, ensuring continued functionality and user safety.

Furthermore, mounting the motor horizontally within the foot was another unlocking decision to achieve a compact design. A similar arrangement was presented in [18] but with no embedded controller and energy source.

However, the current prototype has some limitations. Three out of the four users benefited from a small amount of net mechanical energy from the prosthesis, ranging between 1 and $3\,\mathrm{J}$. In comparison, a healthy human ankle typically generates around $17\,\mathrm{J}$ of net mechanical energy during a gait cycle [39]. This discrepancy indicates room for improvement, which could be addressed through further fine-tuning of the controller. Although we maintained conservative limits on joint assistive torque in this study, both mechanical and thermal analyses suggest that the prosthesis has the capacity to provide significantly higher levels of assistance in future iterations. Nevertheless, targeting 100% might not be desirable since more assistance tends to increase balance issues faced by users with amputation. As a perspective, we believe that enhancing electro-mechanical efficiency may be attainable through fine tuning of the motor driver performance and the mitigation of sources contributing to mechanical losses. Specifically, the limited mechanical energy output observed at higher walking speeds is likely a consequence of the current limitations in motor speed capabilities, itself due to a limitation of the motor driver.

Noise is a significant byproduct of powered devices. A preliminary measurement of the noise produced by ELSA was performed and peak levels ranged from 60 to $65\,\mathrm{dB}$. These values are slightly above those mentioned in [38], ranging from 50 to $60\,\mathrm{dB}$ at approximately $1.5\,\mathrm{m}$, and in [43], ranging from 40 to $55\,\mathrm{dB}$ at $1\,\mathrm{m}$. Such noise levels can cause discomfort to the user in daily life. At the present design stage, minimal attention has been dedicated to noise reduction. Efforts will be paid to mitigate this by fully enclosing the actuation and transmission system, akin to commercial products. Furthermore, the precise balancing of rotary components and the implementation of effective insulation measures to dampen vibrations could also be beneficial.

Another limitation is that the parallel spring design does not allow the ankle joint to rest in a dorsiflexed position. To address tasks requiring a more dorsiflexed neutral position, such as sit-to-stand transfer, the active stiffness feature, designed to compress the parallel spring, can be leveraged. The obvious limitation being the energy consumption required to have the motor work against the spring, but mitigated by the short duration of such events. This trade-off needs to be quantified in the future.

Also, compared to a sound ankle, our device exhibits a relatively limited range of motion, i.e. from 12° in dorsiflexion to 20° in plantarflexion. It is suitable for most tasks but as shown, we reach the limits during stairs ambulation. This is a trade-off resulting from our very compact implementation. However, users with amputation tend to exhibit a lower range of motion than sound individuals [44], decreasing the impact of this design choice.

Finally, it is also worth noting that we included a fixed spring in this design for the sake of simplicity but our previous simulations [29] suggest that implementing a lockable parallel spring might be even more beneficial. This spring would engage earlier after heel strike and harvest more mechanical energy from the motion. We are currently finalizing the design of such a mechanism.

VIII. Conclusion

This work tackled the task of designing and validating a powered ankle-foot prosthesis, ELSA (Efficient and Lightweight Spring Ankle), addressing the need for a lightweight and low build height design. This was achieved leveraging the combination of a spring and motor working in parallel, unlocking the benefits of a low gear ratio, good backdrivability and low reflected inertia. The architecture is hybrid, offering users the choice to receive a varying amount of assistance depending on the task. Some activities, such as ramp descent, can even recharge the battery. The device can also be used completely passively, ensuring continued functionality if the battery is depleted. The prosthesis was validated first on a test bench, quantifying its performance in a controlled environment. Then, experiments were conducted with four users with amputation across different daily-life locomotion activities. The device was able to replicate the ankle dynamics across those scenarios, supplying a net mechanical energy to the user when needed. The influence of several parameters on the resulting performance was evaluated. Further work will address the limitations of the current prototype, improving on the provided assistance and noise generation. A characterization of the custom battery pack will be undertaken. New features, such as stiffness modulation and toe lift will be evaluated. Finally, the impact of the device on the overall gait quality will need to be assessed through a complete investigation of locomotion biomechanics.

Acknowledgment

We acknowledge employees from Össur hf. (Reykjavik, Iceland) for supporting with fitting and alignment, as well as providing access to the testing facilities. We also acknowledge amputee participants recruited for data collection. **Funding** This research was directly funded by Össur hf. through an industrial grant and did not receive funding from a public agency. **Author contributions** F.H conceived and implemented the prosthesis design. J.E. and F.H performed the experiments. J.E. processed the experimental data. R.R directed the research activities. D.L. organized the experimental sessions, helped in recruiting the users and provided access to the testing facilities. All authors performed the analysis, discussed the results and edited the manuscript and approved the submitted version. **Competing interests** D.L is an employee of Össur hf., the financial sponsor of this work. **Data and material availability** All data needed to support the conclusions of this manuscript are included in the main text or Supplementary Materials.

References

[1] T. R. Dillingham, L. E. Pezzin, and E. J. MacKenzie, "Limb amputation and limb deficiency: epidemiology and recent trends in the United States," *Southern Medical Journal*, vol. 95, no. 8, pp. 875–883, Aug. 2002.

[2] T. R. Vogel, G. F. Petroski, and R. L. Kruse, "Impact of amputation level and comorbidities on functional status of nursing home residents after lower extremity amputation," *Journal of Vascular Surgery*, vol. 59, no. 5, pp. 1323 – 1330.e1, 2014. [Online]. Available: http://www.sciencedirect.com/science/article/pii/S074152141302171X

[3] P. L. Ephraim, T. R. Dillingham, M. Sector, L. E. Pezzin, and E. J. MacKenzie, "Epidemiology of limb loss and congenital limb deficiency: a review of the literature1," *Archives of Physical Medicine and Rehabilitation*, vol. 84, no. 5, pp. 747–761, May 2003. [Online]. Available: http://www.sciencedirect.com/science/article/pii/S0003999302049328

[4] S. R. Wurdeman, P. M. Stevens, and J. H. Campbell, "Mobility Analysis of AmpuTees (MAAT I): Quality of life and satisfaction are strongly related to mobility for patients with a lower limb prosthesis," *Prosthetics and Orthotics International*, vol. 42, no. 5, pp. 498–503, Oct. 2018.

[5] I. Melzer, M. Yekutiel, and S. Sukenik, "Comparative study of osteoarthritis of the contralateral knee joint of male amputees who do and do not play volleyball." *The Journal of rheumatology*, vol. 28, no. 1, pp. 169–172, 2001.

[6] J. M. van Velzen, C. A. van Bennekom, W. Polomski, J. R. Slootman, L. H. van der Woude, and H. Houdijk, "Physical capacity and walking ability after lower limb amputation: a systematic review," *Clinical Rehabilitation*, vol. 20, no. 11, pp. 999–1016, 2006. [Online]. Available: https://doi.org/10.1177/0269215506070700

[7] R. M. Williams, A. P. Turner, M. Orendurff, A. D. Segal, G. K. Klute, J. Pecoraro, and J. Czerniecki, "Does having a computerized prosthetic knee influence cognitive performance during amputee walking?" *Archives of Physical Medicine and Rehabilitation*, vol. 87, no. 7, pp. 989–994, Jul. 2006.

[8] R. Gailey, K. Allen, J. Castles, J. Kucharik, and M. Roeder, "Review of secondary physical conditions associated with lower-limb amputation and long-term prosthesis use." *Journal of Rehabilitation Research & Development*, vol. 45, no. 1, 2008.

[9] H. M. Herr and A. M. Grabowski, "Bionic ankle-foot prosthesis normalizes walking gait for persons with leg amputation," *Proceedings. Biological Sciences / The Royal Society*, vol. 279, no. 1728, pp. 457–464, Feb. 2012.

[10] M. E. Carney, T. Shu, R. Stolyarov, J.-F. Duval, and H. M. Herr, "Design and Preliminary Results of a Reaction Force Series Elastic Actuator for Bionic Knee and Ankle Prostheses," *IEEE Transactions on Medical Robotics and Bionics*, vol. 3, no. 3, pp. 542–553, Aug. 2021.

[11] M. Grimmer, M. Holgate, R. Holgate, A. Boehler, J. Ward, K. Hollander, T. Sugar, and A. Seyfarth, "A powered prosthetic ankle joint for walking and running," *BioMedical Engineering OnLine*, vol. 15, no. 3, p. 141, Dec. 2016. [Online]. Available: https://doi.org/10.1186/s12938-016-0286-7

[12] B. E. Lawson, J. Mitchell, D. Truex, A. Shultz, E. Ledoux, and M. Goldfarb, "A Robotic Leg Prosthesis: Design, Control, and Implementation," *IEEE Robotics & Automation Magazine*, vol. 21, no. 4, pp. 70–81, Dec. 2014. [Online]. Available: http://ieeexplore.ieee.org/lpdocs/epic03/wrapper.htm?arnumber=6955797

[13] T. Elery, S. Rezazadeh, C. Nesler, and R. D. Gregg, "Design and Validation of a Powered Knee–Ankle Prosthesis With High-Torque, Low-Impedance Actuators," *IEEE Transactions on Robotics*, vol. 36, no. 6, pp. 1649–1668, Dec. 2020.

[14] A. F. Azocar, L. M. Mooney, J.-F. Duval, A. M. Simon, L. J. Hargrove, and E. J. Rouse, "Design and clinical implementation of an open-source bionic leg," *Nature Biomedical Engineering*, vol. 4, no. 10, pp. 941–953, Oct. 2020. [Online]. Available: https://www.nature.com/articles/s41551-020-00619-3

[15] P. Cherelle, V. Grosu, L. Flynn, K. Junius, M. Moltedo, B. Vanderborght, and D. Lefeber, "The Ankle Mimicking Prosthetic Foot 3—Locking mechanisms, actuator design, control and experiments with an amputee," *Robotics and Autonomous Systems*, vol. 91, pp. 327–336, May 2017. [Online]. Available: https://www.sciencedirect.com/science/article/pii/S0921889016302974

[16] L. Flynn, J. Geeroms, R. Jimenez-Fabian, B. Vanderborght, and D. Lefeber, "Cyberlegs beta-prosthesis active knee system," in *2015 IEEE International Conference on Rehabilitation Robotics (ICORR)*, 2015, pp. 410–415.

[17] J. Geeroms, L. Flynn, R. Jimenez-Fabian, B. Vanderborght, and D. Lefeber, "Ankle-knee prosthesis with powered ankle and energy transfer for cyberlegs α-prototype," in *Rehabilitation robotics (ICORR), 2013 IEEE int. conf. on*. IEEE, 2013, pp. 1–6.

[18] L. Gabert, S. Hood, M. Tran, M. Cempini, and T. Lenzi, "A Compact, Lightweight Robotic Ankle-Foot Prosthesis: Featuring a Powered Polycentric Design," *IEEE Robotics & Automation Magazine*, vol. 27, no. 1, pp. 87–102, Mar. 2020.

[19] M. Tran, L. Gabert, S. Hood, and T. Lenzi, "A lightweight robotic leg prosthesis replicating the biomechanics of the knee, ankle, and toe joint," *Science Robotics*, vol. 7, no. 72, p. eabo3996, 2022. [Online]. Available: https://www.science.org/doi/abs/10.1126/scirobotics.abo3996

[20] J. Kim, J. Wensman, N. Colabianchi, and D. H. Gates, "The influence of powered prostheses on user perspectives, metabolics, and activity: a randomized crossover trial," *Journal of NeuroEngineering and Rehabilitation*, vol. 18, no. 1, p. 49, Mar. 2021. [Online]. Available: https://doi.org/10.1186/s12984-021-00842-2

[21] E. S. Gardinier, B. M. Kelly, J. Wensman, and D. H. Gates, "A controlled clinical trial of a clinically-tuned powered ankle prosthesis in people with transtibial amputation," *Clinical Rehabilitation*, vol. 32, no. 3, pp. 319–329, Mar. 2018.

[22] R. S. Gailey, M. A. Wenger, M. Raya, N. Kirk, K. Erbs, P. Spyropoulos, and M. S. Nash, "Energy expenditure of trans-tibial amputees during ambulation at self-selected pace," *Prosthetics and Orthotics International*, vol. 18, no. 2, pp. 84–91, 1994.

[23] I. A. Mulder, H. R. Holtslag, L. F. Beersma, and B. F. Koopman, "Keep moving forward: A new energy returning prosthetic device with low installation height after syme or pirogoff amputation," *Prosthetics and Orthotics International*, vol. 38, no. 1, pp. 12–20, 2014, pMID: 23625837. [Online]. Available: https://doi.org/10.1177/0309364613485112

[24] J. D. Smith and P. E. Martin, "Effects of prosthetic mass distribution on metabolic costs and walking symmetry," *Journal of Applied Biomechanics*, vol. 29, no. 3, pp. 317–328, Jun. 2013.

[25] Y. S. Narang, V. N. M. Arelekatti, and A. G. Winter, "The Effects of Prosthesis Inertial Properties on Prosthetic Knee Moment and Hip

Energetics Required to Achieve Able-Bodied Kinematics," *IEEE Transactions on Neural Systems and Rehabilitation Engineering*, vol. 24, no. 7, pp. 754–763, Jul. 2016, conference Name: IEEE Transactions on Neural Systems and Rehabilitation Engineering.

[26] L. Gabert, M. Tran, and T. Lenzi, "Design of an Underactuated Powered Ankle and Toe Prosthesis," in *2021 43rd Annual International Conference of the IEEE Engineering in Medicine & Biology Society (EMBC)*, Nov. 2021, pp. 4920–4923.

[27] M. A. Holgate, J. K. Hitt, R. D. Bellman, T. G. Sugar, and K. W. Hollander, "The sparky (spring ankle with regenerative kinetics) project: Choosing a dc motor based actuation method," in *2008 2nd IEEE RAS EMBS International Conference on Biomedical Robotics and Biomechatronics*, Oct 2008, pp. 163–168.

[28] G. A. Pratt and M. M. Williamson, "Series elastic actuators," in *Proceedings 1995 IEEE/RSJ International Conference on Intelligent Robots and Systems. Human Robot Interaction and Cooperative Robots*, vol. 1, Aug 1995, pp. 399–406 vol.1.

[29] F. Heremans and R. Ronsse, "Design of an energy efficient transfemoral prosthesis using lockable parallel springs and electrical energy transfer," in *2017 International Conference on Rehabilitation Robotics (ICORR)*, July 2017, pp. 1305–1312.

[30] F. Heremans, B. Dehez, and R. Ronsse, "Design and validation of a lightweight adaptive and compliant locking mechanism for an ankle prosthesis," in *2018 7th IEEE International Conference on Biomedical Robotics and Biomechatronics (Biorob)*, Aug 2018, pp. 94–99.

[31] F. Heremans, M. Bouri, S. Vijayakumar, B. Dehez, and R. Ronsse, "Bio-inspired design and validation of the efficient lockable spring ankle (elsa) prosthesis," in *16th IEEE/RAS-EMBS International Conference on Rehabilitation Robotics*, Jun 2019.

[32] A. Jurca, J. Žabkar, and S. Džeroski, "Analysis of 1.2 million foot scans from North America, Europe and Asia," *Scientific Reports*, vol. 9, no. 1, p. 19155, Dec. 2019, publisher: Nature Publishing Group. [Online]. Available: https://www.nature.com/articles/s41598-019-55432-z

[33] B. Hordacre, C. Barr, and M. Crotty, "Use of an Activity Monitor and GPS Device to Assess Community Activity and Participation in Transtibial Amputees," *Sensors*, vol. 14, no. 4, pp. 5845–5859, Apr. 2014, number: 4 Publisher: Multidisciplinary Digital Publishing Institute. [Online]. Available: https://www.mdpi.com/1424-8220/14/4/5845

[34] M. R. Tucker, J. Olivier, A. Pagel, H. Bleuler, M. Bouri, O. Lambercy, J. d. R. Millán, R. Riener, H. Vallery, and R. Gassert, "Control strategies for active lower extremity prosthetics and orthotics: a review," *Journal of NeuroEngineering and Rehabilitation*, vol. 12, no. 1, p. 1, Jan 2015. [Online]. Available: https://doi.org/10.1186/1743-0003-12-1

[35] J. Evrard, F. Heremans, and R. Ronsse, "Validation of a heuristic intention detection algorithm for a powered ankle prosthesis across various ambulation tasks," *IEEE EMB's 10th International Conference on Biomedical Robotics and Biomechatronics (BioRob)*, 2024.

[36] J. Camargo, A. Ramanathan, W. Flanagan, and A. Young, "A comprehensive, open-source dataset of lower limb biomechanics in multiple conditions of stairs, ramps, and level-ground ambulation and transitions," *Journal of Biomechanics*, vol. 119, p. 110320, Apr. 2021. [Online]. Available: https://www.sciencedirect.com/science/article/pii/S0021929021001007

[37] J. Evrard, F. Heremans, and R. Ronsse, "On the usability of polymer-based artificial tendons for elastic energy storage in active ankle prostheses," in *2023 International Conference on Rehabilitation Robotics (ICORR)*, 2023, pp. 1–6.

[38] T. Elery, S. Rezazadeh, C. Nesler, and R. D. Gregg, "Design and validation of a powered knee–ankle prosthesis with high-torque, low-impedance actuators," *IEEE Transactions on Robotics*, vol. 36, no. 6, pp. 1649–1668, 2020.

[39] D. A. Winter, *Biomechanics and Motor Control of Human Movement*. John Wiley & Sons, Oct. 2009, google-Books-ID: _bFHL08IWfwC.

[40] A. N. Lay, C. J. Hass, and R. J. Gregor, "The effects of sloped surfaces on locomotion: A kinematic and kinetic analysis," *Journal of Biomechanics*, vol. 39, no. 9, pp. 1621 – 1628, 2006. [Online]. Available: http://www.sciencedirect.com/science/article/pii/S0021929005002150

[41] R. Riener, M. Rabuffetti, and C. Frigo, "Stair ascent and descent at different inclinations," *Gait & Posture*, vol. 15, no. 1, pp. 32–44, Feb. 2002.

[42] Y. Feng, J. Mai, S. K. Agrawal, and Q. Wang, "Energy Regeneration From Electromagnetic Induction by Human Dynamics for Lower Extremity Robotic Prostheses," *IEEE Transactions on Robotics*, vol. 36, no. 5, pp. 1442–1451, Oct. 2020, conference Name: IEEE Transactions on Robotics.

[43] G. Fu, J. Zhu, Z. Wang, J. Mai, and Q. Wang, "Mechatronic design and implementation of a low-noise powered knee prosthesis with high backdrivability," *IEEE/ASME Transactions on Mechatronics*, vol. 28, no. 6, pp. 3180–3190, 2023.

[44] T. Schmalz, S. Blumentritt, and B. Marx, "Biomechanical analysis of stair ambulation in lower limb amputees," *Gait Posture*, vol. 25, no. 2, pp. 267–278, 2007. [Online]. Available: https://www.sciencedirect.com/science/article/pii/S0966636206000531

François Heremans received the B.Sc. and M.Sc. in electromechanical engineering with focus on robotics from UCLouvain, Louvain-la-Neuve, Belgium in 2013 and 2015 repectively. He also received the Ph.D. from the same university in 2019. After being a Postdoctoral Fellow with EPFL, he joined the Institute of Mechanics, Materials and Civil Enginnering (iMMC), UCLouvain. His research interests include the design and control of mechatronic systems for assistance and rehabilitation.

Jeanne Evrard received the B.Sc. and M.Sc. in mechanical engineering from UCLouvain, Louvain-la-Neuve, Belgium in 2018 and 2020 repectively. She is currently working toward the Ph.D. degree at the Institute of Mechanics, Materials and Civil Enginnering (iMMC), also at UCLouvain. Her research interests include the control and validation of mechatronic systems for assistance and rehabilitation.

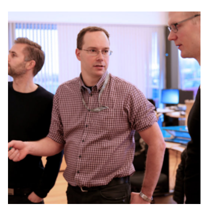

David Langlois received the B.Sc.A. from Université Laval in 1999 and the MASc from the University of British Columbia in 2002, both in mechanical engineering. After holding several positions in research and development at Victhom Human Bionics and Össur hf, he is currently Össur's Center for New Technologies Vice-President. His research interests revolve around powered lower-limb prosthetic and their control systems.

Renaud Ronsse received the M.S. and Ph.D. degrees in engineering from the Université de Liège in 2002 and 2007, respectively. After being a Postdoctoral Fellow with KULeuven and EPFL, he was an Assistant Professor in 2011 then a Professor in 2018 with the Institute of Mechanics, Materials, and Civil Engineering, UCLouvain. He is interested in the transfer of principles governing neural control of human movements into human-centered robotics. His main application fields are bioinspired assistive and rehabilitation robotics, mainly for the lower-limb, and humanoid robotics. More recently, he started a collaborative research to unveil the efficiency optimization mechanisms deployed by biological swimmers and flyers.